Available online at www.sciencedirect.com
SCIENCE DIRECT
Polymer 46 (2005) 1709–1716
polymer
www.elsevier.com/locate/polymer

Crystallization and coalescence of block copolymer micelles in semicrystalline block copolymer/amorphous homopolymer blends

Jun-Ting Xu*, Wei Jin, Guo-Dong Liang, Zhi-Qiang Fan

Department of Polymer Science and Engineering, Zhejiang University, 38 Zheda Road, Hangzhou 310027, China

Received 20 September 2004; received in revised form 5 December 2004; accepted 7 December 2004
Available online 13 January 2005

Abstract

Crystallization of two oxyethylene/oxybutylene block copolymers ($E_{76}B_{38}$ and $E_{155}B_{76}$) from micelles in block copolymer/amorphous homopolymer blends was studied by differential scanning calorimetry (DSC) and time-resolved small angle X-ray scattering (SAXS). Unlike the simultaneous crystallization and formation of superstructure in crystallization from an ordered structure, crystallization of block copolymer from micelles can be divided into two steps. The core of the micelles firstly crystallizes individually, with first-order crystallization kinetics and homogeneous nucleation mechanism. The SAXS revealed that crystallization-induced deformation occurs for the micelles, which strongly depends on microstructure of the block copolymers. For the shorter block copolymer $E_{76}B_{38}$, larger deformation induced by crystallization was observed, leading to coalescence of the micelles after crystallization, while for the longer block copolymer $E_{155}B_{76}$ the micelles show little deformation and the morphology of micelle is retained after crystallization.

Keywords: Crystallization; Micelle; Block copolymer

1. Introduction

Crystallization of block copolymers from the melt with an ordered structure, including lamellae, cylinder and sphere, has been well studied and it has been found that crystallization can be confined either by a glassy wall or by a rubbery wall with strong segregation strength [1–8]. Comparatively, in breakout crystallization coalescence of different micro-domains occurs, which is usually accompanied by the formation of superstructure [9–24]. So far, the structural factors that govern crystallization of block copolymer have been known. The occurrence of confined crystallization in crystalline/rubbery block copolymer is related to the segregation strength and morphology of the block copolymer. The block copolymer with sphere morphology is most likely to exhibit confined crystallization behavior [16,18]. Weakly segregated block copolymers and the block copolymers with the crystalline block as the major component usually exhibit breakout crystallization behavior. However, how coalescence of different micro-domains in breakout crystallization proceeds has not been well understood and some questions remain un-resolved. Firstly, crystallization and coalescence of different micro-domains proceed simultaneously? Usually crystallization and formation of superstructure take place at the same time, but it is not certain that this holds true under all situations. Secondly, coalescence of different micro-domains involves well-separated domains and need to overcomes the unfavorable interaction between the unlike blocks. The effect of kinetic factor such as diffusion on crystallization behavior of block copolymer is still unclear.

In this paper we blended oxyethylene/oxybutylene diblock copolymers (E_mB_n) with large amount of amorphous poly(oxybutylene). Micelles, instead of ordered structure, are formed in the melt of the blends. The aim of the present work is to investigate whether there is any difference in crystallization from the ordered domains and from disordered micelles for the block copolymers. On the other hand, since the distance among crystalline domains in such blends is larger than that in the block copolymers with

* Corresponding author. Tel./fax: +86 571 87952400.
E-mail address: xujt@zju.edu.cn (J.-T. Xu).

0032-3861/$ - see front matter © 2005 Elsevier Ltd. All rights reserved.
doi:10.1016/j.polymer.2004.12.023

ordered structure, the present study can help us understand whether confined crystallization of crystalline/rubbery block copolymers is kinetically trapped due to diffusion factor. Moreover, we have previously reported the crystallization behavior of oxyethylene/oxybutylene diblock copolymers in *n*-hexane, the selective solvent for the amorphous oxybutylene block, using time-resolved SAXS/WAXS [25]. It was found that spherical micelles are retained after crystallization for longer block copolymer $E_{155}B_{76}$, but macro-aggregation takes place for the shorter block copolymer $E_{76}B_{38}$. Nevertheless, it is inconvenient to study crystallization kinetics using DSC due to the presence of solvent. In this paper, the solvent was replaced by the amorphous component and the crystallization kinetics can be readily studied using DSC. To our best knowledge, following two aspects in the present work are novel and have not been reported in literature: the structural change of the micelles induced by crystallization and crystallization kinetics of block copolymer from micelles.

2. Experimental

2.1. Materials

The synthesis and characterization of poly(oxyethylene)-*block*-poly(oxybutylene) copolymers, E_mB_n (here E and B represent oxyethylene block and oxybutylene block, and *m* and *n* denote the polymerization degrees of the two blocks.), used for blending have been described in previous work [26,27]. Both $E_{76}B_{38}$ and $E_{155}B_{76}$ have narrow molecular weight distributions ($M_w/M_n < 1.05$). The PBO homopolymer (B_h) with $M_n = 2000$ (B_{28}) was purchased from Aldrich and was used without further purification. The other PBO homopolymer with $M_n = 1000$ (B_{14}) was specially synthesized by anionic polymerization. Both PBO homopolymers have narrow molecular weight distributions.

2.2. Preparation of the blends

The blends of E_mB_n with B_h were prepared by a solution blending method employing dicholoromethane as solvent. To ensure that PBO homopolymer was miscible with PBO segments in block copolymers and the condition of 'wet brush' was met [28,29], the molecular weight of PBO homopolymer was smaller than half that of PBO block. As a result, $E_{76}B_{38}$ was blended with B_{14} and $E_{155}B_{76}$ was blended with B_{28}. The blends were dried under vacuum for 24 h at 60 °C after the solvent was evaporated, then were cooled to room temperature slowly and stored below 0 °C for usage.

2.3. Time-resolved small angle X-ray scattering

The simultaneous time-resolved SAXS/DSC experiments were carried out at beamline 16.1 in SRS at the Daresbury, Warrington, UK. For $E_{76}B_{38}/B_{14}$ blends the distance between the sample and the SAXS detector was 3.5 m but it was 5.0 m for $E_{155}B_{76}/B_{28}$ blends. The samples were cooled from 100 °C at a rate of 10 °C/min with a Linkam DSC equipped with liquid N_2 cooling system. The data were collected in 10 s frames separated by a waiting-time of 10 μs. Details of the instrument and data processing are described elsewhere [26,27].

2.4. DSC measurements

Non-isothermal crystallization of the blends was performed on a Perkin–Elmer Pyris-1 calorimeter. Samples of the blends about 10 mg were sealed with aluminum pans and were held at 70 °C for 5 min, and then cooled down to −50 °C at a rate of 10 °C/min. The crystallized samples were heated to 70 °C at a rate of 10 °C/min. The thermal lag was ignored and not corrected.

In isothermal crystallization experiments the blends were held at 70 °C for 5 min, and then cooled down at a nominal rate of 100 °C/min to the crystallization temperatures and held until crystallization was completed. The change of heat flow with time was recorded upon crystallization. The isothermal crystallization kinetics of polymer can be analyzed using Avrami equation: [30]

$$1 - X(t) = \frac{\Delta H^c_{t=\infty} - \Delta H^c_t}{\Delta H^c_{t=\infty} - \Delta H^c_{t=0}} = \exp(-kt^n) \quad (1)$$

where $X(t)$ is the relative crystallinity at time t, $\Delta H^c_{t=\infty}$ and ΔH^c_t are the crystallization enthalpies on complete crystallization and after time t. Therefore, we have:

$$\log[-\ln(1 - X(t))] = \log k + n \log t \quad (2)$$

The crystallization rate constant k and Avrami exponent n can be determined from the interception and the slope, respectively, in the plot of $\log[-\ln(1 - X(t))]$ versus $\log(t)$.

3. Results

3.1. DSC results

The non-isothermal crystallization curves and subsequent melting behavior of $E_{76}B_{38}/B_{14}$ blends beyond the order composition are depicted in Figs. 1 and 2, respectively. It is observed that crystallization peaks appear at both higher temperature and lower temperature in the blends with larger volume fraction of the E block, ϕ_E ($\phi_E = 0.12$, 0.10 and 0.08), which fall into the temperature ranges of heterogeneous nucleation and homogeneous nucleation, respectively [17]. This shows that these three blends exhibit fractionated crystallization behavior [31,32]. Because the number of crystallizable domains is far larger than the number of heterogeneous nuclei, heterogeneous nuclei can

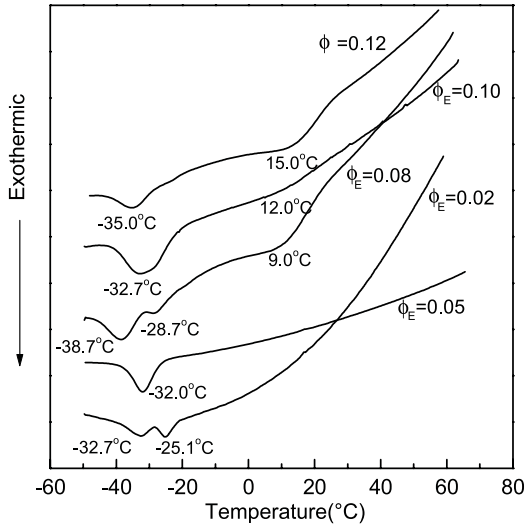

Fig. 1. Non-isothermal crystallization DSC traces of $E_{76}B_{38}/B_{14}$ blends. The cooling rate is 10 °C/min and the volume fractions of E are indicated.

only initiate crystallization of partial domains on decrease of temperature and other domains crystallize via a homogeneous nucleation mechanism. As ϕ_E becomes smaller, only crystallization peaks at lower temperature are observed, indicating that only homogeneous nucleation occurs. All these $E_{76}B_{38}/B_{14}$ blends have melting temperatures not far below that of pure poly(ethylene oxide) (Fig. 2). As a result, the extremely low T_c means larger supercooling for crystallization of the blends with lower ϕ_E. It is also noticed that some blends, for example, at $\phi_E=0.08$ and $\phi_E=0.02$, exhibit double crystallization peaks at low temperature range (below −20 °C). It is tentatively ascribed to the non-uniform size of the crystalline domains. Since the $E_{76}B_{38}/B_{14}$ blend with $\phi_E=0.05$ (E76-005) shows only single crystallization peak at lower temperature, this blend was selected for detailed investigation, including isothermal crystallization and SAXS. The Avrami plots of E76-005 at various crystallization temperatures are illustrated in Fig. 3. It is found that this blend has an Avrami exponent close to $n=1.0$ at all crystallization temperatures studied. The Avrami exponent $n=1.0$ is one of the characteristics of confined crystallization with homogeneous nucleation and zero-dimensional growth [4,14,15,18].

The non-isothermal crystallization and subsequent melting DSC traces of $E_{155}B_{76}/B_{28}$ with $\phi_E=0.05$ (E155-005) are shown in Fig. 4. It is noticed that this blend also shows single crystallization peak at very low temperature, but the melting peak temperature is quite normal. The Avrami plots of E155-005 are shown in Fig. 5. Again an Avrami exponent close to 1.0 is found for this blend at all crystallization temperatures. Above results suggest that the blends E76-005 and E155-005 show similar crystallization kinetics.

When the crystallization rate is controlled by the rate of homogeneous nucleation, we have: [33,34]

$$k \propto \exp\left[-\frac{8\pi\sigma_e^2\sigma_s(T_m^o)^2}{k_B T_c(\Delta H_f^o)^2(T_m^o - T_c)^2\rho^2}\right] \quad (3)$$

where ΔH_f^o and T_m^o are the heat of fusion and the equilibrium melting temperature for infinite chain length, respectively. T_c is crystallization temperature, ρ designates the density of the crystallized E block and k_B is the Boltzman constant. σ_e and σ_s are the interfacial free energy between crystalline and amorphous regions for the folding surface and lateral surface of crystal nucleus. As a result, a plot of $\ln k$ versus $(T_m^o)^2/[T_c(T_m^o - T_c)^2]$ would yield a straight line and the interfacial free energy can be derived from the slope of this line. Such plots for E76-005 and E155-005 are shown in Fig. 6. It is observed that there is indeed a linear relationship between $\ln k$ and $(T_m^o)^2/[T_c(T_m^o - T_c)^2]$, verifying that the

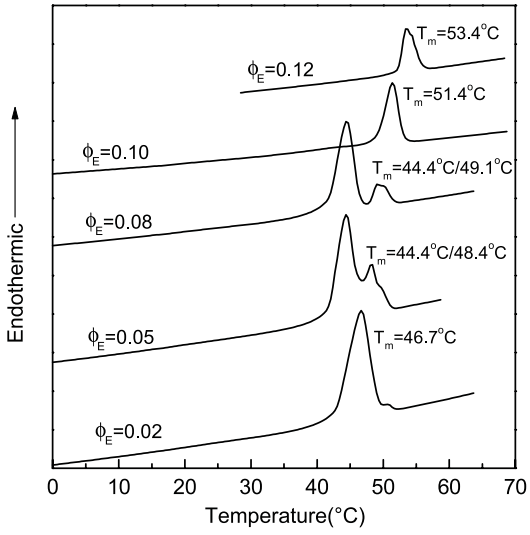

Fig. 2. Melting DSC traces of $E_{76}B_{38}/B_{14}$ blends after non-isothermal crystallization. The heating rate is 10 °C/min and the volume fractions of E are indicated.

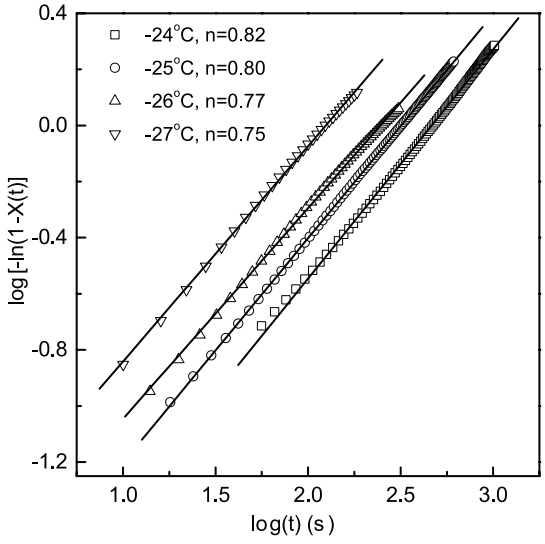

Fig. 3. Avrami plots for $E_{76}B_{38}/B_{14}$ ($\phi_E=0.05$) crystallized at various temperatures.

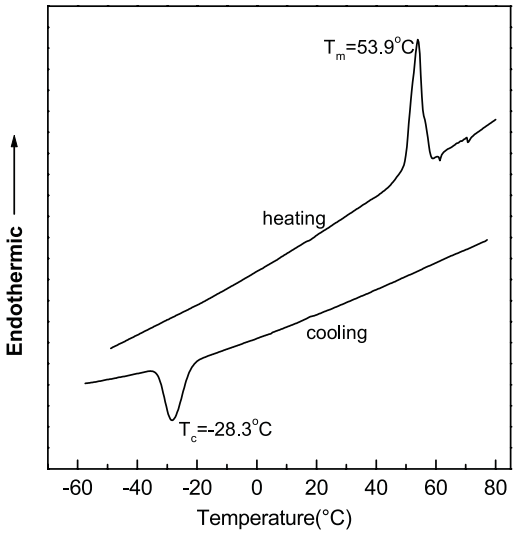

Fig. 4. Non-isothermal crystallization and subsequent melting DSC traces of $E_{155}B_{76}/B_{28}$ ($\phi_E=0.05$) blend. The cooling and heating rates are 10 °C/min.

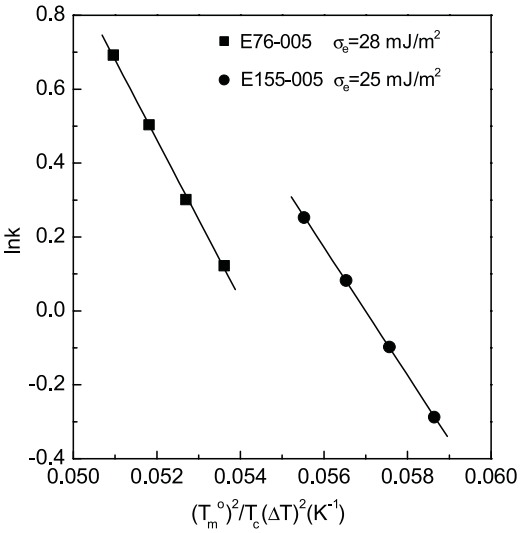

Fig. 6. Plots of $\ln k$ versus $(T_m^o)^2/[T_c(T_m^o-T_c)^2]$ for isothermal crystallization of $E_{76}B_{38}/B_{14}$ ($\phi_E=0.05$) (E76-005) and $E_{155}B_{76}/B_{28}$ ($\phi_E=0.05$) (E155-005).

crystallization rates of E76-005 and E155-005 are controlled by the rate of homogeneous nucleation. The values of 208 J/g, 343 K and 1.23 g/cm^3 are used for ΔH_f^o, T_m^o and ρ, respectively, for both blends. Assuming that the value of σ_s is 10 mJ/m^2 [35], the values of σ_e obtained are 28 mJ/m^2 and 25 mJ/m^2 for E76-005 and E155-005, respectively. These values are slightly smaller than those for crystallization confined in ordered domains [18].

3.2. Time-resolved SAXS

Fig. 7 shows the SAXS profiles of E76-005 cooled from 100 °C at a rate of 10 °C/min. It found that the SAXS peak is very weak and broad at 100 and 80 °C. This peak is associated with the characteristic concentration fluctuations, indicating a mean-field disordered state [36]. From 60 °C the first-order SAXS peak becomes obvious as temperature decreases and another weak second-order peak appears around $q=0.12\sim0.10$ Å^{-1}. For the purpose of clarity, a single SAXS profile at −25 °C is shown in Fig. 8. One can see from Fig. 8 that the second-order peak does exist

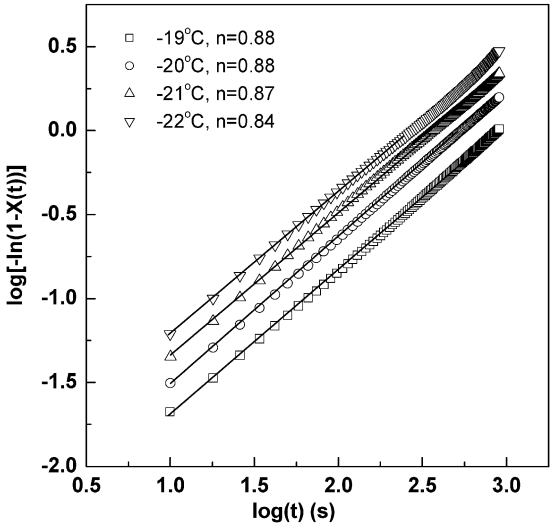

Fig. 5. Avrami plots for $E_{155}B_{76}/B_{28}$ ($\phi_E=0.05$) crystallized at various temperatures.

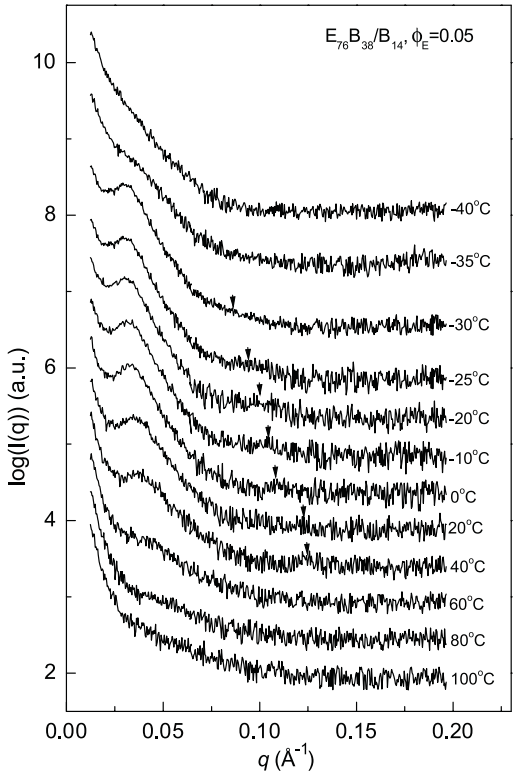

Fig. 7. SAXS profiles of $E_{76}B_{38}/B_{14}$ ($\phi_E=0.05$) cooled from 100 °C at a rate of 10 °C/min. Each SAXS profile is shifted up by 0.5. The arrows indicate the scattering arising from form factor of the micelles.

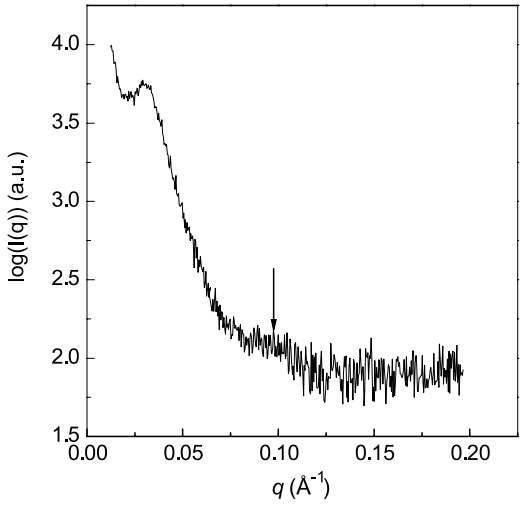

Fig. 8. SAXS profile of $E_{76}B_{38}/B_{14}$ (ϕ_E=0.05) at −25 °C.

though its intensity is quite low. Recently, micellization/demicellization transition above order-disorder transition temperature (T_{ODT}) has been reported for the block copolymers with highly asymmetric composition [37–40]. The presence of micelles without long-range order led to a second-order SAXS peak due to form factor scattering of the micelles. The second-order SAXS peak in E76-005 can also be ascribed to formation of micelles, though this blend has disordered morphology in the solid state. The micellization/demicellization transition temperature (T_{DMT}) can be determined by the plot of inversion of the intensity of the first-order SAXS peak ($1/I_{max}$) versus inversion of temperature ($1/T$) [37,38]. As shown in Fig. 9, T_{DMT} is the temperature at which two lines cross. The T_{DMT} is about 60 °C for E76-005. When temperature is lower than −30 °C, the SAXS peaks move to lower q and tend to disappear. Most importantly, the second-order SAXS peak arising from form factor of the micelles cannot be observed. It should be emphasized that the disappearance of SAXS peak

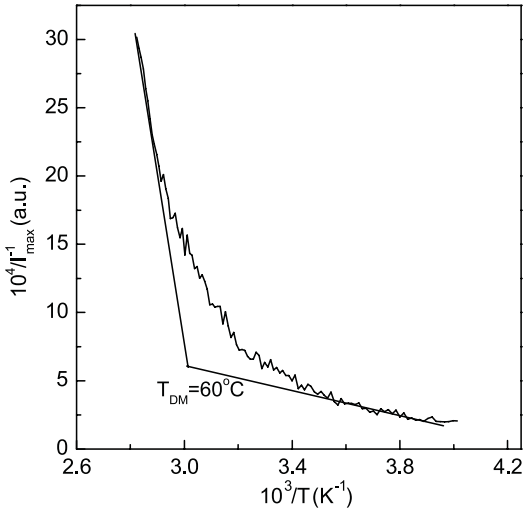

Fig. 9. Plot of $1/I_{max}$ versus $1/T$ for E76-005.

at lower temperature is not due to the homogeneous blend, but due to coalescence of the micelles. Since the domain size of the E block becomes larger after aggregation but the volume fraction of the E block remains unchanged, the distance among the macro-crystals is out of the measurement range of SAXS experiment. The formation of macro-crystals is supported by the fact that the blend becomes cloudy after crystallization. The change of SAXS profiles with temperature shows that coalescence of the micelles takes place in the blend E76-005 after crystallization.

The SAXS profiles of E155-005 during cooling are shown in Fig. 10. It is noticed that the first-order SAXS peaks of E155-005 are partially overlapped with beamstop, though the distance between the sample and the SAXS detector is 5.0 m, which is the upper limit of this beamline. The second-order SAXS peak is also overlapped with the first-order peak, which broadens the SAXS peaks. Although the SAXS profiles of E155-005 exhibit low resolution, we can still see some differences between Fig. 7 and Fig. 10. A most striking feature of Fig. 10 is that the SAXS profiles hardly change with temperature. Both the first- and the second SAXS peaks, which result from structure factor and form factor of the micelles, respectively, nearly keep unchanged in the temperature range from 100 to −40 °C. This shows that in E155-005 micelles have been formed even at 100 °C and the micelles are retained after crystallization. We also notice that E155-005 remains transparent after crystallization.

4. Discussion

In combination with crystallization kinetics and SAXS results, we can deduce how E_mB_n block copolymers crystallize from the micelles in the blends. The first-order crystallization

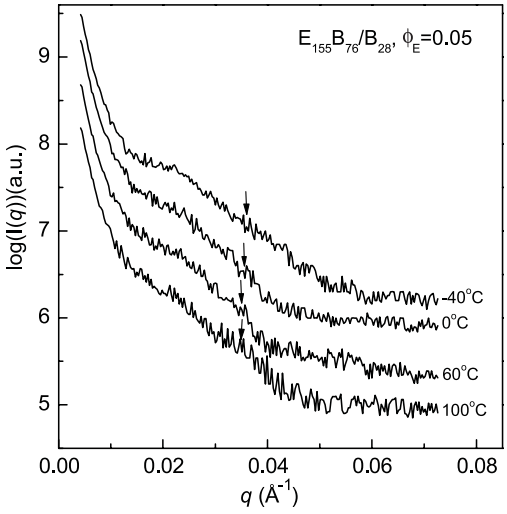

Fig. 10. SAXS profiles of $E_{155}B_{76}/B_{28}$ (ϕ_E=0.05) cooled from 100 °C at a rate of 10 °C/min. Each SAXS profile is shifted up by 0.5. The arrows indicate the scattering arising from form factor of the micelles.

kinetics and homogeneous nuclea-tion mechanism show that the micelles composed of poly(oxyethylene) blocks in both E76-005 and E155-005 first crystallize individually and there is on interference among the micelles. Otherwise, larger Avrami exponent should have been observed. Since the number of the micelles is far larger than that of heterogeneous nuclei, crystallization initiated by heterogeneous nuclei can be ignored and homogeneous nucleation occurs for the blends. As a result, the blends crystallize at very low temperature, which is similar to crystallization of polymers well dispersed in the dilute [41–45]. However, the shift of the SAXS peak to lower q in E76-005 shows that coalescence of the micelles happens after crystallization. Therefore, crystallization of micelles and coalescence of the micelles do not proceed simultaneously. This result shows that the crystallization mechanisms of block copolymer from micelles and from ordered micro-phase separated morphologies are quite different. When breakout crystallization occurs for the block copolymers from ordered micro-phase separated morphology, crystallization and rupture of morphology usually take place simultaneously, leading to a large Avrami exponent. This observation also shows that the first order crystallization kinetics and homogeneous nucleation are only characteristics of confined crystallization, but not always related with preservation of morphology after crystallization, as pointed in our previous work [46]. By contrast, the unchanged SAXS patterns of E155-005 during crystallization indicate that the micelles are preserved after crystallization. The radius of the spherical micelles (R) can be estimated from the form factor $P(q,R)$ when the effect of the structure factor is ignored:

$$P(q,R) = \left[\frac{3(\sin(qR) - qR\cos(qR))}{(qR)^3}\right]^2 \quad (4)$$

The form factor $P(q,R)$ exhibits a maximum at $qR = 5.76$ and the values of R can be obtained from the maximum of the form factor. The changes of R with temperature during cooling are illustrated in Fig. 11. It should be noted that the values of R obtained for E76-005 and E155-005 are not accurate due to the low resolution and weak intensity of the second-order peak in the SAXS profiles. It is found that the values of R for the micelles in E155-005 keep around 160 Å in the temperature range studied and show little change before and after crystallization. This shows that the micelle morphology is retained after crystallization and little deformation occurs for the micelles of E155-005 due to crystallization. In contrast, the values of R for the micelles of E76-005 increase from 47 Å at 60 °C to 65 Å at −25 °C and R cannot be calculated at temperature lower than −25 °C due to absence of the second-order peak associated with form factor, showing that the micelles in E76-005 undergo large deformation during crystallization. Following the deformation, coalescence of the micelles takes place in E76-005 and macro-crystals are formed. In summary, the

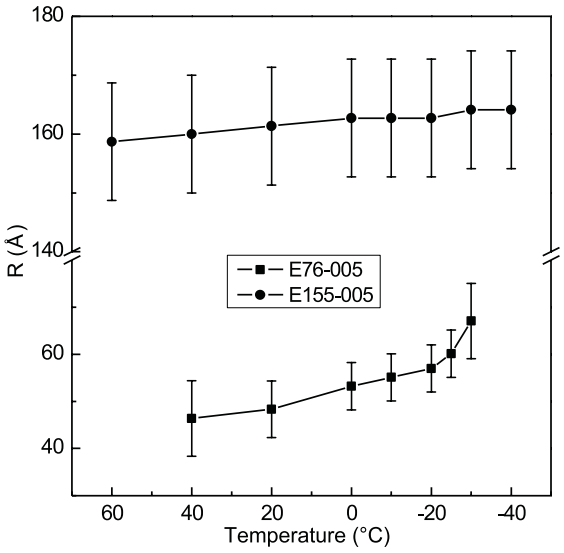

Fig. 11. Change of radius of the micelles during cooling.

crystallization process and subsequent morphological change for E76-005 and E155-005 can be represented by Fig. 12. It must be emphasized that such a sequence of crystallization and coalescence of the micelles is only applicable to single micelles. Because different micelles crystallize at different times and coalescence of micelle occurs immediately after crystallization, the overall crystallization process of the blends may proceed simultaneously accompanied by coalescence of the micelles. As a result, simultaneous SAXS/WAXS experiment is helpless to probe the crystallization mechanism of block copolymer from the micelles. For this reason, we did not observe the appearance of WAXS peak prior to the change of SAXS profiles when E_mB_n block copolymers crystallize from micelles in n-hexane solution [25].

Based on the radius of the micelles and the volume fraction of the poly(oxyethylene) block, the average distance between two adjacent micelles, L, can be estimated. The values of L are 125 Å and 380 Å, respectively, for

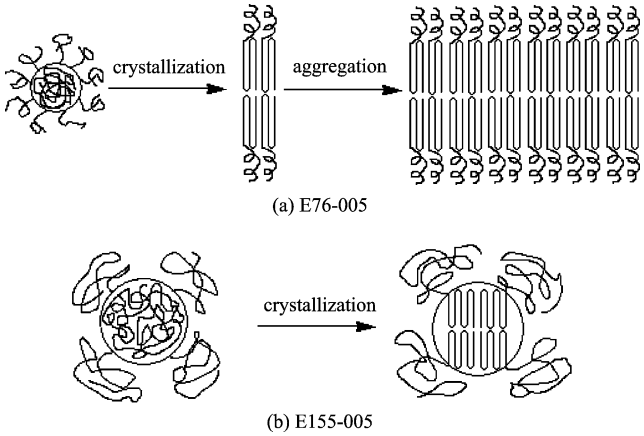

Fig. 12. Schematics for crystallization and morphological change in E76-005 and E155-005.

E76-005 and E155-006. We notice that the distance of 125 Å in E76-005 is larger that in $E_{155}B_{76}/B_{28}$ blend with $\phi_E = 0.18$ and sphere morphology, which is 117 Å [17]. Our previous work revealed that the $E_{155}B_{76}/B_{28}$ blend with $\phi_E = 0.18$ exhibits confined crystallization behavior [17,18], but macro-aggregation is still observed in E76-005. This shows that the distance between two crystalline domains, i.e. diffusion, is not the major factor governing crystallization behavior of the block copolymers.

So far we have studied crystallization of E_mB_n block copolymers from ordered melt [18], from micelles in E_mB_n/B_h blends and from micelles in *n*-hexane solution [25]. Although the mechanisms of crystallization from ordered micro-phase separated morphologies and from micelles are different, a similar phenomenon is observed: the morphology before crystallization is destroyed for shorter block copolymer $E_{76}B_{38}$ after crystallization, but it is retained for the longer block copolymer $E_{155}B_{76}$. The effect microstructure of the block copolymers on crystallization behavior can be explained from the viewpoint of free energy. There are three major parts that contribute to the total free energy: the fusion enthalpy of the crystalline block, the conformation entropy of the amorphous and the interfacial free energy [47–49]. The morphology of the block copolymer is determined by the balance of these three major contributions. The blend of the shorter block copolymer, E76-005, forms smaller micelles and thus have larger interfacial free energy. To reduce the interfacial free energy the micelles tend to deform and aggregate after crystallization (Fig. 12(a)). On the other hand, the shorter amorphous block has a smaller amount of conformation and has minor contribution to the total free energy. This allows larger deformation of the amorphous block without an evident increase in free energy. Moreover, the shorter blocks have stronger mobility, which makes the aggregation easier. As a result, in the E76-005 aggregation of the micelles after crystallization tends to take place in both thermodynamic and kinetics. In contrast, when the block copolymer becomes longer, the amorphous block has a larger contribution to the total free energy. In order to obtain large conformation entropy, the amorphous block adopts coiled conformation rather than highly stretched conformation. If the micelles aggregate, the amorphous blocks have to be stretched, resulting in increase of free energy. The random-coiled amorphous blocks with long length also cover the lateral interface and hinder the coalescence of different micelles (Fig. 12(b)).

5. Conclusions

The crystallization kinetics and SAXS results show that crystallization of the E block from the micelles in E_mB_n/B_h blends can be divided into two steps: Firstly, the micelles crystallize individually through homogeneous nucleation. Secondly, crystallization induces deformation of the micelles. The extent of deformation is strongly dependent on microstructure of the block copolymers. For shorter block copolymer larger deformation occurs and the deformed micelles can aggregate into macro-crystals, while the micelles of the longer E_mB_n block copolymer undergo little deformation and the morphology of micelle is retained after crystallization.

Acknowledgements

Prof. C. Booth in University of Manchester and Prof. A.J. Ryan in The University of Sheffield are greatly acknowledged for providing the block copolymers and helpful discussion. This project was supported by National Natural Science Foundation of China (20374046) and by the Excellent Young Teachers Program of MOE.

References

[1] Cohen RE, Cheng PL, Douzinas K, Kofinas P, Berney CV. Macromolecules 1990;23:324.
[2] Sakurai K, MacKnight WJ, Lohse DJ, Schulz DN, Sissano JA, Lin JS, et al. Polymer 1996;37:4443.
[3] Weimann PA, Hajduk DA, Chu C, Chaffin KA, Brodil JC, Bates FS. J Polym Sci Part B: Polym Phys 1999;37:2053.
[4] Chen HL, Wu JC, Lin TL, Lin JS. Macromolecules 2001;34:6936.
[5] Chen HL, Li HC, Huang YY, Chiu FC. Macromolecules 2002;35:2417.
[6] Huang YH, Yang CH, Chen HL, Chiu FC, Lin TL, Liou W. Macromolecules 2004;37:486.
[7] Zhu L, Cheng SZD, Calhoun BH, Ge Q, Quirk RP, Hsiao BS, Yeh FJ. Chin J Polym Sci 2000;18:287.
[8] Zhu L, Cheng SZD, Calhoun BH, Ge Q, Quirk RP, Thomas EL, Hsiao BS, Yeh FJ, Lotz B. J Am Chem Soc 2000;122:5957.
[9] Zhu L, Mimnaugh BR, Ge Q, Quirk RP, Cheng SZD, Thomas EL, et al. Polymer 2001;42:9121.
[10] Zhu L, Cheng SZD, Calhoun BH, Ge Q, Quirk RP, Thomas EL, Hsiao BS, Yeh F, Lotz B. Polymer 2001;42:5829.
[11] Reiter G, Castelein G, Sommer JU, Rottele A, Thurn-Albrecht T. Phys Rev Lett 2001;87:226101.
[12] Rottele A, Thurn-Albrecht T, Sommer JU, Reiter G. Macromolecules 2003;36:1257.
[13] Shiomi T, Tsukada H, Takeshita H, Takenaka K, Tezuka Y. Polymer 2001;42:4997.
[14] Loo YL, Register RA, Ryan AJ. Phys Rev Lett 2000;84:4120.
[15] Loo YL, Register RA, Ryan AJ, Dee GT. Macromolecules 2001;34:8968.
[16] Loo YL, Register RA, Ryan AJ. Macromolecules 2002;35:2365.
[17] Xu JT, Turner SC, Fairclough JPA, Mai SM, Ryan AJ, Chaibundit C, Booth C. Macromolecules 2002;35:3614.
[18] Xu JT, Fairclough JPA, Mai SM, Ryan AJ, Chaibundit C. Macromolecules 2002;35:6937.
[19] Xu JT, Yuan JJ, Cheng SY. Eur Polym J 2003;39:2091.
[20] Ueda M, Sakurai K, Okamoto S, Lohse DJ, MacKnight WJ, Shinkai S, Sakurai S, Nomura S. Polymer 2003;44:6995.
[21] Shiomi T, Imai K, Takenaka K, Takeshita H, Hayashi H, Tezuka Y. Polymer 2001;42:3233.
[22] Albuerne J, Marquez L, Muller AJ, Raquez JM, Degee P, Dubois P. Macromolecules 2003;36:1633.

[23] Floudas G, Reiter G, Lambert O, Dumas P. Macromolecules 1998;31:7279.
[24] Kim G, Han CC, Libera M, Jackson CL. Macromolecules 2001;34:7336.
[25] Xu JT, Fairclough JPA, Mai SM, Ryan AJ. J Mater Chem 2003;13:2740.
[26] Mai SM, Fairclough JPA, Viras K, Gorry PA, Hamley IW, Ryan AJ, Booth C. Macromolecules 1997;30:8392.
[27] Mai SM, Fairclough JPA, Terrill NJ, Turner SC, Hamley IW, Matsen MW, Ryan AJ, Booth C. Macromolecules 1998;31:8110.
[28] Tanaka H, Hasegawa H, Hashimoto T. Macromolecules 1991;24:240.
[29] Winey KI, Thomas EL, Fetters LJ. Macromolecules 1992;25:2645.
[30] Avrami M. J Chem Phys 1939;7:1103.
[31] Balsamo V, Muller AJ, von Gyldenfeldt F, Stadler R. Macromol Chem Phys 1998;199:1063.
[32] Muller AJ, Balsamo V, Arnal ML, Jakob T, Schmalz H, Abetz V. Macromolecules 2002;35:3048.
[33] Uhlmann DR, Kritchevsky G, Straff R, Scherer G. J Chem Phys 1975;62:4896.
[34] Wunderlich B. Crystal nucleation, growth, annealing. In: Macromolecular physics, vol. 2. London: Academic Press; 1976.
[35] Richardson PH, Richards RW, Blundell DJ, Macdonald WA, Mills P. Polymer 1995;36:3059.
[36] Leibler L. Macromolecules 1980;13:1602.
[37] Kim JK, Lee HH, Sakurai S, Aida S, Masamoto J, Nomura S, Kitagawa Y, Suda Y. Macromolecules 1999;32:6707.
[38] Han CD, Vaidya NY, Kim D, Shin G, Yamaguchi D, Hashimoto T. Macromolecules 2000;33:3767.
[39] Dormidontova EE, Lodge TP. Macromolecules 2001;34:9143.
[40] Wang XH, Dormidontova EE, Lodge TP. Macromolecules 2002;35:9687.
[41] Cormia RL, Price FP, Turnbull D. J Chem Phys 1962;37:1333.
[42] Everaert V, Groeninckx G, Aerts L. Polymer 2000;41:1409.
[43] Arnal ML, Muller AJ, Maiti P, Hikosaka M. Macromol Chem Phys 2000;201:2493.
[44] Chen HL, Hsiao SC, Lin TL, Yamauchi K, Hasegawa H, Hashimoto T. Macromolecules 2001;34:671.
[45] Taden A, Landfester K. Macromolecules 2003;36:4037.
[46] Xu JT, Fairclough JPA, Mai SM, Chaibundit C, Mingvanish M, Booth C, Ryan AJ. Polymer 2003;44:6843.
[47] DiMarzio EA, Guttman CM, Hoffmann JD. Macromolecules 1980;13:1194.
[48] Whitmore MD, Noolandi J. Macromolecules 1988;21:1482.
[49] Vilgis T, Halperin A. Macromolecules 1991;24:2090.